

Research Article





MCOFs for CO₂ Photoreduction

Very Important Paper

How to cite: *Angew. Chem. Int. Ed.* **2025**, e202505292 doi.org/10.1002/anie.202505292

Modulating the Chromophores of Metal-Covalent Organic Frameworks for Boosting Low-Concentration CO₂ Photoreduction

Chong-Jiu Lu, Ji-Hong Zhang, Jian-Hua Mei, Yun-Nan Gong,* Tong-Bu Lu, and Di-Chang Zhong*

Abstract: The development of efficient photocatalysts to convert low-concentration CO2 into the valueadded chemicals and fuels is particularly interesting yet remains highly challenging. Herein, we designed and synthesized three metal-covalent organic frameworks (MCOFs) through the Schiff-base condensation reactions between trinuclear copper complex and different BDP-based chromophores (BDP = 4,4-difluoro-4-bora-3a,4a-diaza-s-indacene) for visible-light-driven reduction of low-concentration CO₂ (15%) to HCOO⁻. As a result, MCOF-ANT containing anthracene (ANT) groups achieves the highest HCOO⁻ production rate of 1658 μ mol g⁻¹ h⁻¹ (HCOO⁻ selectivity, ~100%) in the absence of any additional noble-metal photosensitizers under a laboratory light source, which is 7.2 and 2.1 times higher than those of MCOF-Ph and MCOF-Nap with phenyl (Ph) and naphthalene (Nap) groups, respectively. Furthermore, MCOF-ANT also exhibits excellent photocatalytic activity for the reduction of low-concentration CO₂ (15%) to HCOO⁻ under natural sunlight, with a HCOO⁻ production rate of 1239 µmol g⁻¹ h⁻¹ (HCOO⁻ selectivity, ~100%). Experiments and theoretical calculations reveal that the presence of ANT in MCOF-ANT is favorable to the visible-light harvesting and charge separation, as well as the formation of *OCO intermediate, which clearly accounts for its superior catalytic activity.

Introduction

The massive combustion of fossil fuels has led to a dramatic increase of carbon dioxide (CO_2) emission in the atmosphere, which caused serious energy and climate crisis.^[1-6] Photocatalytic reduction of CO_2 into the value-added chemicals and fuels has been recognized as a promising approach to mitigate the above two issues.^[7-12] In the past decade, a large

[*] C.-J. Lu, J.-H. Zhang, J.-H. Mei, Y.-N. Gong, T.-B. Lu, D.-C. Zhong Institute for New Energy Materials and Low Carbon Technologies, School of Materials Science and Engineering, Tianjin University of Technology, Tianjin 300384, China E-mail: yngong@email.tjut.edu.cn

dczhong@email.tjut.edu.cnAdditional supporting information can be found online in the

number of efficient photocatalysts have been developed for CO_2 reduction, while these photocatalytic systems focused on the reduction of high-concentration CO_2 (>99%). [13–18] Considering the anthropogenic CO_2 pollutants mainly generate from industrial gaseous waste with CO_2 concentration of 5%–15%, the photoreduction of low-concentration CO_2 is more meaningful and closer to reality. [19–22] However, it remains a great challenge to achieve efficient low-concentration CO_2 reduction because of the insufficient efficiency of CO_2 adsorption and activation on the surface of photocatalysts at low CO_2 concentration. Therefore, it is of great significance to develop photocatalytic systems that can effectively enrich and activate low-concentration CO_2 to achieve efficient low-concentration CO_2 reduction.

It is known that an efficient photocatalyst must have excellent light-harvesting ability, high charge separation efficiency and high catalytic efficiency of active sites. In recent years, metal-organic frameworks (MOFs) constructed by metal ions/clusters and organic linkers via coordination bonds,[23-26] and covalent organic frameworks (COFs) assembled through covalent bonding of conjugated organic building blocks, [27-35] have been widely applied as photocatalysts for CO₂ reduction due to their well-defined and tailorable structures, high surface area and desired semiconductor-like behavior. However, both of them exhibit insufficient photocatalytic activity because MOFs usually display poor visible-light-harvesting capability and COFs often lack metal catalytic sites. To conquer these, covalent bonding of metal complexes and conjugated organic building blocks to form metal-covalent organic frameworks (MCOFs) is expected to integrate the abundant metal sites of MOFs and excellent visible-light absorption ability of COFs in a single photocatalytic system to improve catalytic activity.[36-40] Furthermore, a series of strategies have been developed to enhance photocatalytic performance of MOFs and COFs, among which the introduction of organic conjugated groups in the skeletons to regulate their chromophores has been considered as an effective strategy because it can improve both light-harvesting capability and charge separation efficiency. [41-44] Nevertheless, the investigations on chromophores regulation for boosting photocatalytic CO₂ reduction activity remain extremely rare.

Considering this, we rationally fabricated three MCOFs by covalent bonding of trinuclear copper complex and different BDP-based chromophores (BDP = 4,4-difluoro-4-bora-3a,4a-diaza-s-indacene) for photocatalytic CO_2 reduction. Under visible-light irradiation, these MCOFs exhibit high catalytic activity for the reduction of low-concentration CO_2 (15%)

Additional supporting information can be found online in the Supporting Information section

15213773, 0, Downloaded from https://onlinelibrary.wiley.com/doi/10.1002/anie.20250522 by Tianjin University Of, Wiley Online Library on [09.052025]. See the Terms and Conditions (https://onlinelibrary.wiley.com/terms-and-conditions) on Wiley Online Library for rules of use; OA articles are governed by the applicable Creative Commons Licenson

Research Article



 ${\rm CO_2}$ and 85% ${\rm N_2}$) to HCOO⁻, among which the MCOF-ANT with anthracene (ANT) groups displays the largest HCOO⁻ generation rate of 1658 µmol g⁻¹ h⁻¹ in the absence of any additional noble-metal photosensitizers under a laboratory light source, 7.2- and 2.1-fold higher than those of MCOF-Ph and MCOF-Nap with phenyl (Ph) and naphthalene (Nap) groups, respectively. Moreover, MCOF-ANT also exhibits high photocatalytic low-concentration ${\rm CO_2}$ reduction performance under natural sunlight, with a HCOO⁻ generation rate of 1239 µmol g⁻¹ h⁻¹. Such high photocatalytic activity of MCOF-ANT is attributed to its outstanding visible-light harvesting capacity and charge separation efficiency, as well as low energy barrier of the rate-determining step for ${\rm CO_2}$ photoreduction, as demonstrated by a series of control experiments and theoretical calculations.

Results and Discussion

The trinuclear copper complex Cu-CTC-NH₂ (CTC = cyclic trinuclear complex) and BDP-based chromophores (BDP-X, X = Ph, Nap and ANT) were synthesized according to reported procedures.^[45,46] The powder X-ray diffraction (XRD) pattern of synthesized Cu-CTC-NH2 is in good agreement with that of simulated one, demonstrating the successful synthesis of the expected structure (Figure S1). The results of ¹H and ¹³C nuclear magnetic resonance (NMR) spectra demonstrate that BDP-X chromophores are successfully obtained with high purity (Figures S2–S7). Afterward, the Schiff-base condensation reactions between Cu-CTC-NH₂ and BDP-X were conducted to produce three MCOFs (named MCOF-X, X = Ph, Nap and ANT) (Figure 1a,b). The formation of a Schiff base linkages in MCOF-X were confirmed by Fourier transform infrared spectroscopy (FTIR) and ¹³C solid-state NMR spectroscopy (¹³C ssNMR). In the FTIR spectra, the C=O stretching vibration bands of MCOF-X at approximately 1670 cm⁻¹ disappear, while the strong characteristic C=N stretching vibrations at approximately 1626 cm⁻¹ are observed, verifying the formation of imine linkages (Figures 1c, S8 and S9).[47,48] Furthermore, the ¹³C ssNMR spectra of MCOF-X show the characteristic carbon signals of the C=N bonds at approximately 156 ppm, further validating the presence of imine linkages (Figures 1d, S10 and S11).[49] The SEM images of MCOF-X show similar spherical-shaped morphology with diameters of ~ 1 µm (Figures \$12–\$14).

The crystal structures of MCOF-X were determined by powder XRD experiments combined with theoretical structural simulations. As shown in Figures S15–S17, the AA, AB, and ABC stacking models based on MCOF-ANT were built using Materials Studio. The experimental powder XRD pattern of MCOF-ANT matches well with the calculated result for the AA stacking model (Figures 1e and S18). Pawley refinement of MCOF-ANT unveils that it crystallized in the P3 space group with the refined unit cell parameters of a = b = 40.7572 Å, c = 4.5608 Å and residual factor values of $R_p = 1.06\%$ and $R_{wp} = 1.73\%$ (Table S1). MCOF-ANT exhibits one intense diffraction peak at 2.44° , corresponding to the (100) crystal plane. Moreover, two minor peaks at 4.98°

and 8.70° are also observed, which can be attributed to the (200) and (310) crystal planes, respectively (Figure S18). For MCOF-Ph and MCOF-Nap, the experimental powder XRD patterns also match well with the calculated results from the AA stacking model (Figures S19–S26). Pawley refinement was applied to verify the structural models of MCOF-Ph and MCOF-Nap, which provide good residual factors of $R_{\rm p}/R_{\rm wp}=2.94/3.84\%$ and $R_{\rm p}/R_{\rm wp}=2.70/3.57\%$ for MCOF-Ph and MCOF-Nap respectively, implying the validity of the computational models (Figures S27and S28; Tables S2 and S3). The simulated crystal structures of MCOF-X show almost the same pore sizes of ~2.5 nm (Figures 1b, S29, and S30). More details and raw data are given in the Supporting Information.

The porous features of MCOF-X were examined by gas adsorption experiments. The N2 adsorption measurements at 77 K and 1 atm reveal the reversible type IV adsorptiondesorption isotherms with mesoporous nature for MCOF-X (Figure 2a). The Brunauer-Emmett-Teller (BET) surface areas of MCOF-Ph, MCOF-Nap, and MCOF-ANT are calculated to be 271, 224, and 155 m² g⁻¹, respectively. Moreover, they exhibit almost the same pore sizes of ~ 2.5 nm, which agree well with the theoretical results (Figures 1b and \$29-\$33). Additionally, the N₂ adsorption isotherms of MCOF-X at 298 K and 1 atm demonstrate that MCOF-X can hardly absorb N₂ molecules (Figures S34–S36). However, the results of N₂/CO₂ (85% N₂ and 15% CO₂) adsorption isotherms show that MCOF-Ph, MCOF-Nap, and MCOF-ANT display almost the same gas adsorption capacities of \sim 5.0 cm³ g⁻¹ at 298 K and 1 atm (Figures S34–S36), suggesting that MCOF-X can absorb CO2 molecules at low concentration, which would be beneficial for the low-concentration CO₂ reduction. The optical absorption properties and band gaps of MCOF-X were investigated by solid-state UV-vis spectra. As shown in Figure 2b, all MCOF-X exhibit strong lightharvesting ability in the UV and visible light regions. It's worth noting that the intrinsic absorption edges of MCOF-X gradually red-shift with increasing the conjugated degree of X groups, revealing that the introduction of organic conjugated groups in the skeletons of MCOFs improves the visiblelight harvesting capacity. The band gaps (E_{o}) of MCOF-Ph, MCOF-Nap and MCOF-ANT are estimated to be 1.49, 1.50, and 1.50 eV respectively based on their Tauc plots (Figures S37-S39). Furthermore, Mott-Schottky measurements of MCOF-X were performed to study their band positions. The flat band potentials of MCOF-Ph, MCOF-Nap, and MCOF-ANT were determined to be -0.87, -0.92, and -0.84 V versus NHE, respectively, which are equal to their conduction band (CB) potentials (Figures 2c and \$40-\$41). Therefore, their valence band (VB) positions were accordingly calculated to be 0.62, 0.58, and 0.66 V versus NHE respectively based on the equation $E_{\rm g}=E_{\rm VB}-E_{\rm CB}$ (Figure 2d). Obviously, MCOF-X are thermodynamically suitable for photocatalytic CO₂ reduction because their CB potentials are more negative compared with some CO₂ photoreduction products (HCOO⁻, -0.61 V; CO, -0.52 V; CH₄, -0.24 V; versus NHE at pH = 7).[50–56]

Encouraged by the above results, the photocatalytic CO₂ reduction experiments of MCOF-X have been carried out

15213773, 0, Downloaded from https://onlinelibrary.wiley.com/doi/10.1002/anie.20250522 by Tianjin University Of, Wiley Online Library on [09.052025]. See the Terms and Conditions (https://onlinelibrary.wiley.com/terms-and-conditions) on Wiley Online Library for rules of use; OA articles are governed by the applicable Creative Commons Licenson

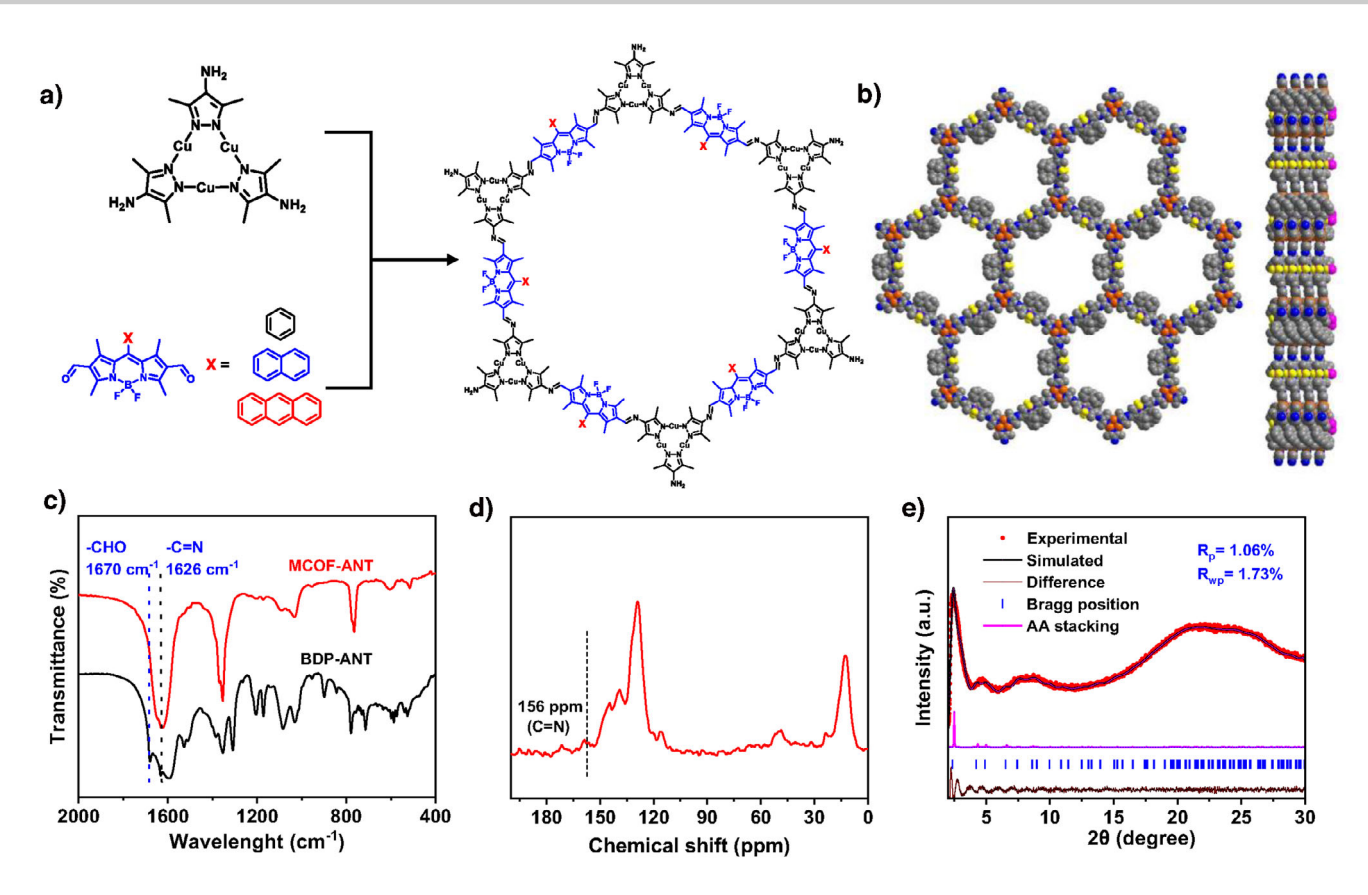


Figure 1. a) Schematic of the synthesis of MCOF-X (X = Ph, Nap or ANT) through the Schiff-base condensation reactions between trinuclear copper complex and different BDP-based chromophores. b) The two-dimensional layer and three-dimensional stacking structures of MCOF-ANT. c) FT-IR spectra of BDP-ANT and MCOF-ANT. d) ¹³C ssNMR of MCOF-ANT. e) Experimental (red dot) and simulated (black line) powder XRD patterns of MCOF-ANT.

under visible light irradiation (300 W Xe lamp with a cut-off filter of 420 nm) with CH_3CN/H_2O (v:v = 4:1) as the solvent and 1,3-dimethyl-2-phenylbenzimidazoline (BIH) as the sacrificial electron donor, without adding any additional noblemetal photosensitizers. As shown in Figures \$42 and \$43, the MCOF-X with slight variation in the chromophores exhibit significantly different photocatalytic activities for the photoreduction of CO₂ to HCOO⁻. Among which, MCOF-ANT with the largest conjugated group achieves the highest HCOOgeneration rate of 2288 μ mol g⁻¹ h⁻¹, which is 7.1 and 2.3 times higher than those of MCOF-Ph and MCOF-Nap, respectively. Furthermore, no other reduction product other than HCOO- was detected in the catalytic system of MCOF-X, indicating that the HCOO⁻ selectivities of them are nearly 100%. The apparent quantum yields (AQYs) of MCOF-X were measured at 450 and 530 nm, and the change of AQYs for the three photocatalysts is consistent with the tendency of their photocatalytic performance, in which the largest AQY of MCOF-ANT reaches as high as 1.59% at 450 nm (Figure S44). In addition, we further evaluate the photocatalytic performance of MCOF-ANT under natural sunlight. As shown in Figure S45, MCOF-ANT still exhibits excellent catalytic activity under sunny day with HCOO- generation rate of 1809 μ mol g⁻¹ h⁻¹ (HCOO⁻ selectivity, ~100%).

Given that MCOF-X exhibit outstanding photocatalytic activities in >99% CO₂ atmosphere, the low-concentration

CO₂ (15% CO₂ and 85% N₂) photoreduction of them were further studied. Under visible light irradiation, MCOF-ANT still shows a high HCOO- generation rate of 1658 μ mol g⁻¹ h⁻¹ (HCOO⁻ selectivity, ~100%) without any additional noble-metal photosensitizers under a laboratory light source, which is also significantly higher than those of MCOF-Ph (229 µmol g⁻¹ h⁻¹) and MCOF-Nap (776 μ mol g⁻¹ h⁻¹) (Figure 3a). The high catalytic activity of MCOF-X at low-concentration CO2 may be attributed to two aspects: 1) MCOF-X exhibit excellent selective adsorption characteristics for CO₂ in mixed gas (Figures S34-S36); 2) The open copper sites in MCOF-X can strongly bind with CO₂, not only facilitating the CO₂ adsorption but also reinforcing the CO₂ activation, as reported for Cu-CTC-NH₂.^[57,58] Moreover, the AQYs of MCOF-X in low-concentration CO₂ were obtained at 450 and 530 nm, respectively. As shown in Figure 3b, they exhibit different AQYs at the tested wavelengths, following the sequence of MCOF-ANT > MCOF-Nap > MCOF-Ph, among which the AQY of MCOF-ANT is 0.44% at 450 nm. These results further indicate that the regulation of chromophores in MCOFs by altering organic conjugated groups plays an important role in modulating photocatalytic CO₂ reduction performance. It's also worth noting that the photocatalytic activity for low-concentration CO₂ reduction of MCOF-ANT is superior to many reported photocatalysts at low-concentration CO₂

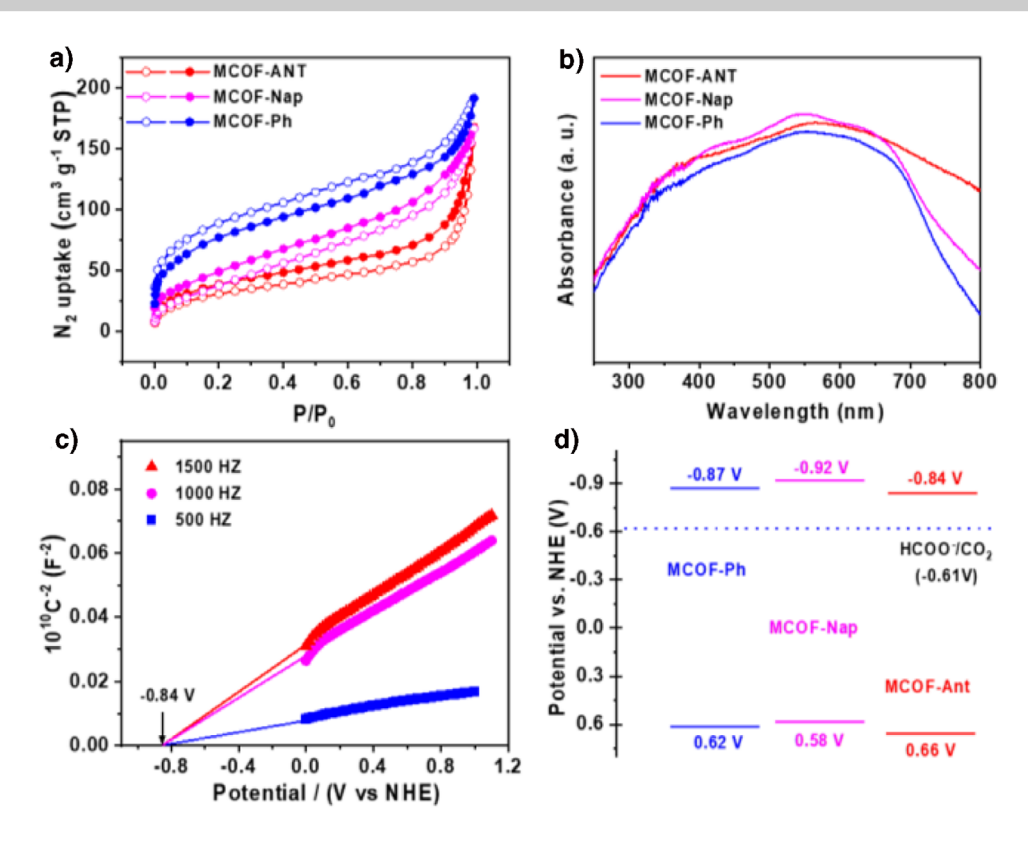


Figure 2. a) N₂ adsorption-desorption isotherms for MCOF-X at 77 K. b) Solid-state UV-vis spectra of MCOF-X. c) Mott-Schottky plots of MCOF-ANT. d) Band-structure diagrams for MCOF-X.

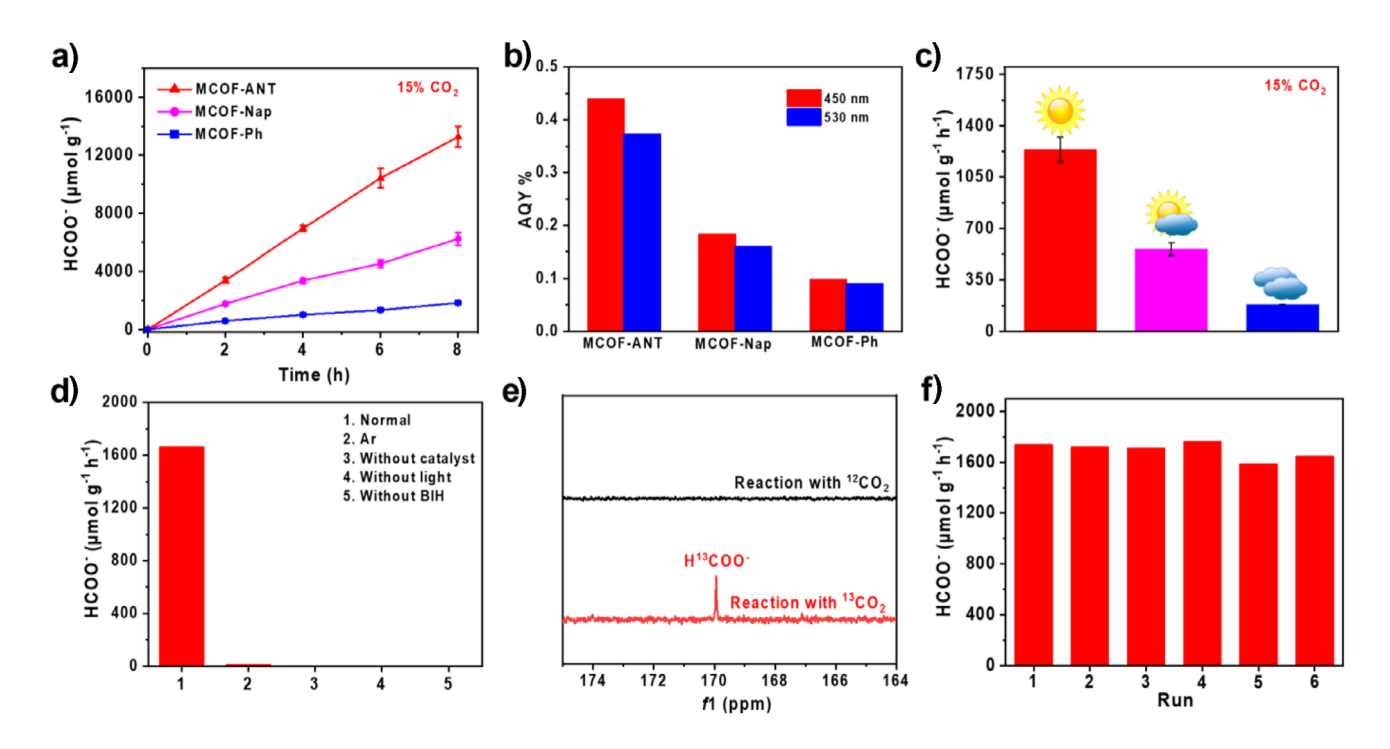


Figure 3. a) The amount of HCOO $^-$ produced over MCOF-ANT under visible light irradiation and 15% CO $_2$ /85% N $_2$ atmosphere. b) The AQY values of MCOF-X under 15% CO $_2$ and 85% N $_2$ atmosphere. c) The photocatalytic HCOO $^-$ production rate of MCOF-ANT under natural sunlight and 15% CO $_2$ /85% N $_2$ atmosphere. d) The control experiments of photocatalytic CO $_2$ reduction performance over MCOF-ANT under 15% CO $_2$ and 85% N $_2$ atmosphere. e) 13 C NMR spectra of the liquid product obtained from the photocatalytic CO $_2$ reduction over MCOF-ANT using 13 CO $_2$ instead of 12 CO $_2$. f) The photocatalytic HCOO $^-$ production rate of MCOF-ANT in six consecutive runs under 15% CO $_2$ and 85% N $_2$ atmosphere.

1521373, Q. Downloaded from https://onlinelibrary.wielyc.com/doi/10.002/anie.20250522 by Tianjin University Of, Wiley Online Library on [09.052025]. See the Terms and Conditions (https://onlinelibrary.wielyc.com/terms-and-conditions) on Wiley Online Library for rules of use; OA articles are governed by the applicable Creative Commons Licensea

Research Article

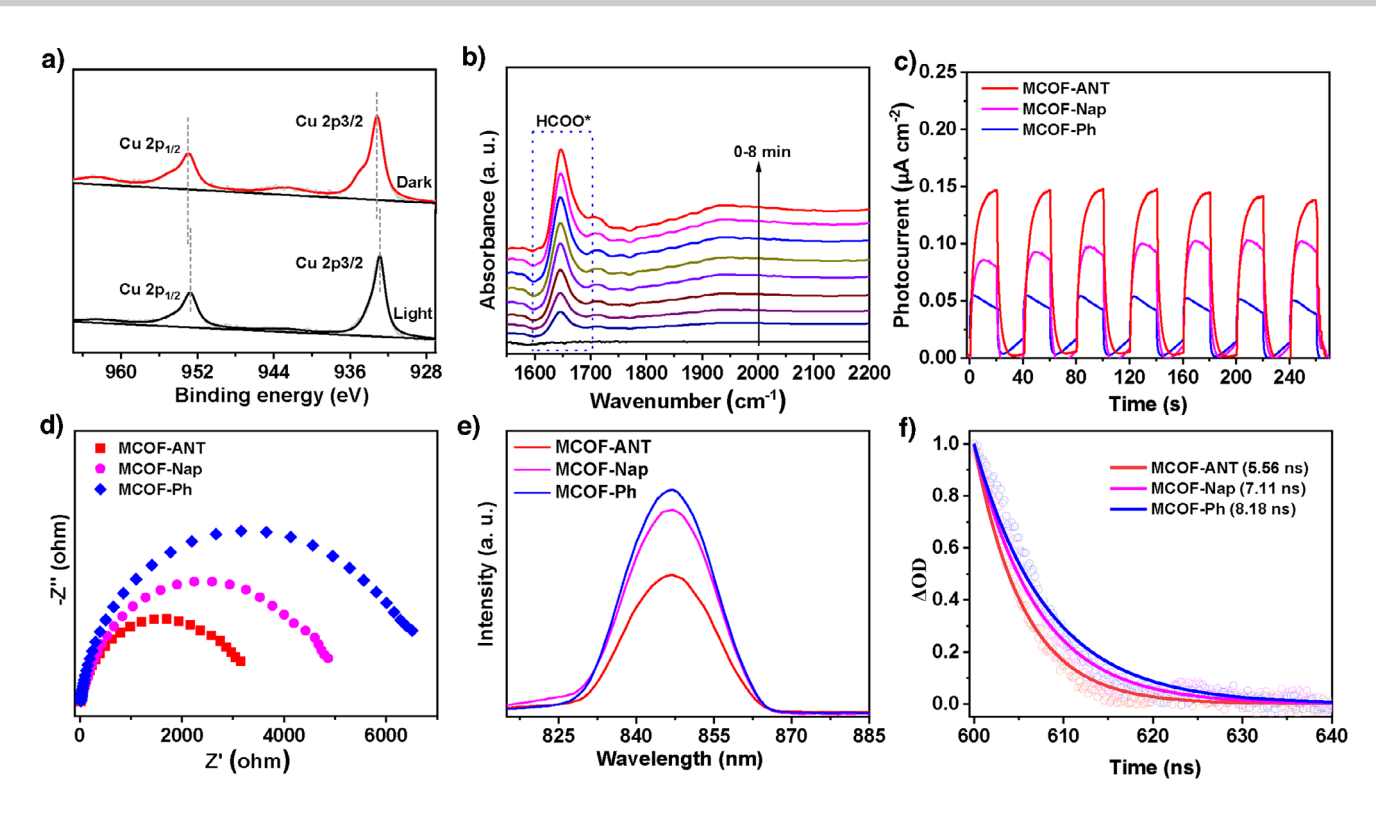


Figure 4. a) XPS spectra of Cu 2p in the dark and under light irradiation for MCOF-ANT. b) In situ FTIR spectra of MCOF-ANT. c) Photocurrent response of MCOF-X. d) EIS spectra of MCOF-X. e) PL spectra of MCOF-X. f) TA spectra of MCOF-X.

atmosphere (Table S4). Additionally, the low-concentration CO_2 photoreduction for MCOF-ANT was also conducted under natural sunlight. The HCOO⁻ generation rate and selectivity of MCOF-ANT are 1239 μ mo g⁻¹ h⁻¹ and \sim 100% under sunny day, respectively (Figure 3c). All the above observations demonstrate that MCOF-ANT indeed has a high performance for low-concentration CO_2 photoreduction, which is closer to practical industrial application.

In the control experiments over MCOF-ANT, negligible amounts of CO₂ reduction products are detected in the absence of photocatalyst, BIH, CO₂, or light irradiation, demonstrating that these factors are indispensable to the lowconcentration CO₂ photoreduction (Figure 3d). Moreover, a low-concentration ¹³CO₂ isotope trace experiment of MCOF-ANT was carried out to validate the carbon source of HCOO-. As shown in Figure 3e, the ¹³C NMR spectrum displays an obvious signal at 169.8 ppm, which can be attributed to the H¹³COO⁻.[59] These results unambiguously confirm that the generated HCOO- indeed originates from CO2 photoreduction. Subsequently, the photocatalytic durability of MCOF-ANT for low-concentration CO₂ photoreduction was evaluated by consecutive recycling experiments, with each cycle for 8 h. It was observed that no discernible decrease in HCOO- generation rate, indicative of the excellent stability of MCOF-ANT (Figure 3f). Powder XRD pattern and UV-vis spectra also indicate that the structural integrity of MCOF-ANT can be well kept during the catalytic reaction (Figures \$46 and \$47).

The possible mechanism for CO₂ photoreduction over MCOF-ANT was elucidated by in situ X-ray photoelectron

spectroscopy (XPS) measurement. The results show that the Cu $2p_{3/2}$ and Cu $2p_{1/2}$ binding energies locate at 933.1 and 952.9 eV in the dark, which display negative shift to 932.8 and 952.7 eV respectively upon light irradiation, hinting that Cu obtains electrons in the photocatalytic process (Figure 4a).

Moreover, the binding energy of B shows positive shift upon light irradiation compared with that in the dark, implying that BDP-ANT loses electrons (Figure \$48). Therefore, it is proposed that the BDP-ANT chromophores in MCOF-ANT harvests visible light to generate electrons and holes, where electrons are transferred to the Cu to reduce CO₂, and holes are annihilated by sacrificial agent BIH. Moreover, in situ fourier transform infrared spectroscopy (FTIR) measurements of MCOF-ANT were conducted to detect the key intermediates in the process of CO₂ photoreduction. As shown in Figure 4b, a new infrared absorption peak at 1647 cm⁻¹ was detected for MCOF-ANT, which can be assigned to the key intermediates of HCOO* for HCOOgeneration. It is worth noting that the intensity of this peak gradually increases with the incremental irradiation time, indicating the increased concentration of HCOO* intermediate during the CO₂ photoreduction. [60-63]

In order to elucidate the enhanced photocatalytic activity of MCOF-ANT compared with MCOF-Ph and MCOF-Nap, the photocurrent response, electrochemical impedance spectroscopy (EIS), photoluminescence (PL) emission spectra and time-resolved PL (TRPL) spectra of MCOF-X were performed. As shown in Figure 4c, all photocatalysts show obvious photocurrent signals, in which the MCOF-ANT exhibits the strongest response intensity, demonstrating that

15213773, 0, Downloaded from https://onlinelibrary.wiley.com/doi/10.1002/anie.20250522 by Tianjin University Of, Wiley Online Library on [09.052025]. See the Terms and Conditions (https://onlinelibrary.wiley.com/terms-and-conditions) on Wiley Online Library for rules of use; OA articles are governed by the applicable Creative Commons Licenson

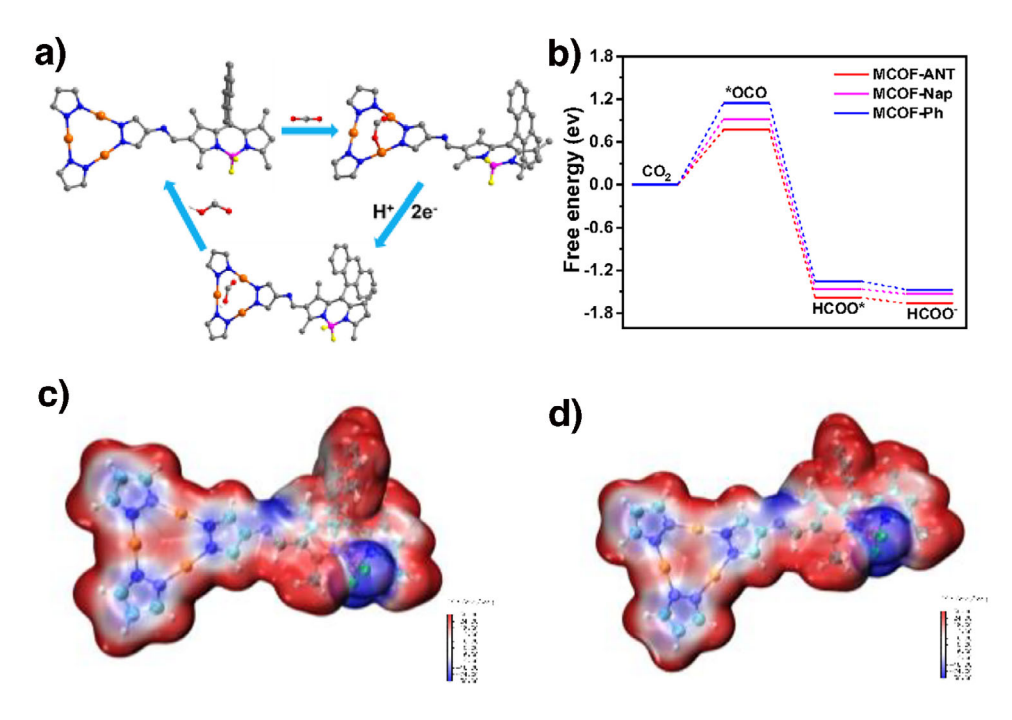


Figure 5. a) Possible mechanism for CO₂ photoreduction to HCOO⁻ over MCOF-ANT. b) Gibbs free energy diagrams for CO₂ photoreduction to HCOO⁻ for MCOF-X. Calculated ESP distribution maps of MCOF-ANT c) and MCOF-Ph (d).

it has the best separation of photo-generated electrons and holes. The results of EIS show that the radius trend of Nyquist plots follows MCOF-ANT < MCOF-Nap < MCOF-Ph, suggesting that MCOF-ANT possesses the fastest electron transfer (Figure 4d). In the PL spectra analysis, MCOF-ANT exhibits the weakest emission intensity among the three MCOFs, implying the most efficient charge separation (Figure 4e). Moreover, the results of TRPL spectra show that the average lifetimes of MCOF-X follow an order of MCOF-ANT < MCOF-Nap < MCOF-Ph, further confirming the most efficient charge separation of MCOF-ANT (Figure \$49). Besides, the transient absorption (TA) spectra of MCOF-X were carried out to investigate charge-separated state. [64-70] As shown in Figures 4f and S50-S52, the strong bleaching signals around 560 nm are observed upon pulsed laser excitation, and the lifetimes of the charge-separated state are found to be 5.56, 7.11, and 8.18 ns for MCOF-ANT, MCOF-Nap, and MCOF-Ph, respectively. These results certify again that MCOF-ANT shows the most efficient charge separation. All the results above reveal that the introduction of large conjugated groups in the chromophores of MCOFs can significantly improve charge separation efficiency, thereby boost the catalytic activity of CO₂ photoreduction.

Density functional theory (DFT) calculations were further performed to elucidate how the photocatalytic CO₂ reduction activity is regulated by varying organic conjugated groups of chromophores in MCOF-X, as well as the origin of the outstanding photocatalytic performance of MCOF-ANT. It is know that photocatalytic CO₂ reduction to HCOO⁻ involves the following steps. First, CO2 is adsorbed at the catalytic site. Second, the adsorbed *CO₂ receives the electron and proton to form HCOO*. Finally, HCOO* desorption occurs to produce HCOO⁻ (Figure 5a). As shown in Figure 5b, the formation of *CO₂ for the reduction of CO₂ to HCOO⁻ is the rate-determining step (RDS) for the three MCOFs. The free-energy change (ΔG) values of RDS for MCOF-ANT, MCOF-Nap, and MCOF-Ph are 0.77, 0.92, and 1.14 eV, respectively. Obviously, MCOF-ANT exhibits the lowest ΔG value of RDS, suggesting that the introduction of the largest conjugated group in the chromophores of MCOFs is the most beneficial for the CO₂ photoreduction to HCOO-. Moreover, the electrostatic surface potential (ESP) of MCOF-X was calculated to study carrier separation efficiency (Figures 5c,d and \$53). In the ESP, blue and red surfaces represent the positive and negative potential regions, respectively. It can clearly see that MCOF-ANT shows the broadest distribution of electrostatic potential among the three MCOFs, demonstrating that MCOF-ANT displays the greatest degree of polarization.^[71-73] This can facilitate the efficient separation of photogenerated carriers and enhance the utilization efficiency of photogenerated electrons, thus improving photocatalytic activity of CO2 reduction. These calculated results are consistent well with the above experimental results, which explain again the highest photocatalytic activity of MCOF-ANT among the three MCOFs.

Conclusion

In summary, three MCOF-X were successfully constructed by covalent bonding of trinuclear copper complex and BDP-based chromophores with different organic conjugated groups, which exhibit outstanding catalytic activities for low-concentration CO2 photoreduction to HCOO-. Among which, MCOF-ANT shows the highest photocatalytic performance with HCOO⁻ generation rate of 15213773, 0, Downloaded from https://onlinelibrary.wiley.com/doi/10.1002/anie.20250522 by Tianjin University Of, Wiley Online Library on [09.052025]. See the Terms and Conditions (https://onlinelibrary.wiley.com/terms-and-conditions) on Wiley Online Library for rules of use; OA articles are governed by the applicable Creative Commons Licenson

15213773, Q. Downloaded from https://onlinelibrary.wiley.com/doi/10.1002/anie.20250522b by Tianjin University Of, Wiley Online Library on [09.052025]. See the Terms and Conditions (https://onlinelibrary.wiley.com/terms-and-conditions) on Wiley Online Library for rules of use; OA articles are governed by the applicable Creative Commons Licensea



1658 umol g⁻¹ h⁻¹ without adding any additional noble-metal photosensitizers under visible light irradiation with a 300 W Xe lamp, which is not only 7.2 and 2.1-fold higher than those of MCOF-Ph and MCOF-Nap respectively, but also superior to many reported photocatalysts at low-concentration CO2 atmosphere. Additionally, MCOF-ANT also displays an impressive catalytic activity for low-concentration CO₂ photoreduction under natural sunlight with HCOOgeneration rate of 1239 µmol g⁻¹ h⁻¹. Experimental and DFT calculation results reveal that the high photocatalytic activity of MCOF-ANT is attributed to the splendid visiblelight harvesting capacity and charge separation efficiency, as well as the low RDS ΔG value for CO₂ photoreduction. This study provides a facile approach to develop efficient catalysts for low-concentration CO₂ photoreduction.

Acknowledgements

This work was supported by National Key R&D Program of China (2022YFA1502902), the National Natural Science Foundation of China (22371208, 22271218), and the Natural Science Foundation of Tianjin City (24JCZDJC00220, 24JCYBJC00800).

Conflict of Interests

The authors declare no conflict of interest.

Data Availability Statement

The data that support the findings of this study are available in the supplementary material of this article.

Keywords: Chromophores · Low-concentration CO₂ reduction · Metal-covalent organic frameworks • Photocatalysis

- [1] S. Lin, C. S. Diercks, Y.-B. Zhang, N. Kornienko, E. M. Nichols, Y.-B. Zhao, A. R. Paris, D. Kim, P.-D. Yang, O. M. Yaghi, C. J. Chang, Science 2015, 349, 1208-1213.
- [2] M. Bonchio, J. Bonin, O. Ishitani, T.-B. Lu, T. Morikawa, A. J. Morris, E. Reisner, D. Sarkar, F. M. Toma, M. Robert, Nat. Catal. 2023, 6, 657-665.
- [3] Z. Jiang, X.-H. Xu, Y.-H. Ma, H. S. Cho, D. Ding, C. Wang, J. Wu, P. Oleynikov, M. Jia, J. Cheng, Y. Zhou, O. Terasaki, T.-Y. Peng, L. Zan, H.-X. Deng, Nature 2021, 590, E16.
- [4] K. Kohse-Höinghaus, Chem. Rev. 2023, 123, 5139–5219.
- [5] J. P. Helveston, G. He, M. R. Davidson, *Nature* **2022**, *612*, 83–87.
- [6] R.-B. Lin, B. Chen, Joule 2018, 2, 1030–1032.
- [7] D.-C. Zhong, Y.-N. Gong, C. Zhang, T.-B. Lu, Chem. Soc. Rev. **2023**, *52*, 3170–3214.
- [8] N. F. Suremann, B. D. McCarthy, W. J. Gschwind, A. Kumar, B. A. Johnson, L. Hammarström, S. Ott, Chem. Rev. 2023, 123, 6545-6611.
- [9] P. Fratzl, Chem. Rev. 2023, 123, 1841–1842.
- [10] R. M. Bullock, J. G. Chen, L. Gagliardi, P. J. Chirik, O. K. Farha, C. H. Hendon, C. W. Jones, J. A. Keith, J. Klosin, S. D. Minteer, R. H. Morris, A. T. Radosevich, T. B. Rauchfuss, N. A. Strotman,

- A. Vojvodic, T. R. Ward, J. Y. Yang, Y. Surendranath, Science 2020, 369, eabc3183.
- J. Chen, R. Abazari, K. A. Adegoke, N. W. Maxakato, O. S. Bello, M. Tahir, S. Tasleem, S. Sanati, A. M. Kirillov, Y. Zhou, Coord. Chem. Rev. 2022, 469, 214664.
- [12] H.-W. Lin, S.-O. Luo, H.-B. Zhang, J.-H. Ye, Joule 2022, 6, 294-
- [13] Q. Li, J.-N. Chang, Z.-M. Wang, M. Lu, C. Guo, M. Zhang, T.-Y. Yu, Y.-F. Chen, S.-L. Li, Y.-Q. Lan, J. Am. Chem. Soc. 2023, 145, 23167-23175.
- [14] K. Sun, Y. Huang, Q.-Y. Wang, W.-D. Zhao, X.-S. Zheng, J. Jiang, H.-L. Jiang, J. Am. Chem. Soc. 2024, 146, 3241-3249.
- [15] W.-L. Wang, C.-L. Ji, K. Liu, C.-G. Zhao, W.-P. Li, J. Xie, Chem. Soc. Rev. 2021, 50, 1874-1912.
- [16] T. Ouyang, H.-J. Wang, H.-H. Huang, J.-W. Wang, S. Guo, W.-J. Liu, D.-C. Zhong, T.-B. Lu, Angew. Chem. Int. Ed. 2018, 57, 16480-16485; Angew. Chem. 2018, 130,16718-16723.
- [17] J.-H. Ding, X.-Y. Guan, J. Lv, X.-H. Chen, Y. Zhang, H. Li, D.-L. Zhang, S.-L. Qiu, H.-L. Jiang, Q.-R. Fang, J. Am. Chem. Soc. **2023**, 145, 3248-3254.
- [18] K. Sun, Y.-Y. Qian, H.-L. Jiang, Angew. Chem. Int. Ed. 2023, 62, e202217565; Angew. Chem. 2022, 135, e202217565.
- [19] Y. Wang, J.-X. Wei, H.-L. Tang, L.-H. Shao, L.-Z. Dong, X.-Y. Chu, Y.-X. Jiang, G.-L. Zhang, F.-M. Zhang, Y.-Q. Lan, Nat. Commun. 2024, 15, 8818.
- [20] M. Dong, J. Zhou, J. Zhong, H.-T. Li, C.-Y. Sun, Y.-D. Han, J.-N. Kou, Z.-H. Kang, X.-L. Wang, Z.-M. Su, Adv. Funct. Mater. **2022**, 32, 2110136.
- [21] J.-H. Liu, B. Han, X.-M. Liu, S.-J. Liang, Y. Fu, J. He, L.-H. Chung, Y.-F. Lin, Y.-P. Wei, S.-B. Wang, T.-Y. Ma, Z.-F. Yang, Angew. Chem. Int. Ed. 2024, e202417435.
- [22] H.-N. Huang, R. Shi, Z.-H. Li, J.-Q. Zhao, C.-L. Su, T.-R. Zhang, Angew. Chem. Int. Ed. 2022, 61, e202200802; Angew. Chem. 2022, 134, e202200802.
- [23] D.-D. Li, M. Kassymova, X.-C. Cai, S.-Q. Zang, H.-L. Jiang, Coord. Chem. Rev. 2020, 412, 213262.
- [24] P. Rassu, X.-J. Ma, B. Wang, Coord. Chem. Rev. 2022, 465, 214561.
- [25] N. A. Nordin, M. A. Mohamed, M. N. I. Salehmin, S. F. Mohd Yusoff, Coord. Chem. Rev. 2022, 468, 214639.
- [26] K. Sun, Y. Huang, F. Sun, Q.-Y. Wang, Y.-J. Zhou, J.-X. Wang, Q. Zhang, X.-S. Zheng, F.-T. Fan, Y. Luo, J. Jiang, H.-L. Jiang, Nat. Chem. 2024, 16, 1638-1646.
- [27] R.-Y. Liu, Y.-Z. Chen, H.-D. Yu, M. Položij, Y.-Y. Guo, T. C. Sum, T. Heine, D.-L. Jiang, Nat. Catal. 2024, 7, 195–206.
- [28] F.-Y. Liu, P. Zhou, Y.-H. Hou, H. Tan, Y. Liang, J.-L. Liang, Q. Zhang, S.-J. Guo, M.-P. Tong, J.-R. Ni, Nat. Commun. 2023, 14, 4344.
- [29] Y.-N. Gong, X.-Y. Guan, H.-L. Jiang, Coord. Chem. Rev. 2023, 475, 214889.
- [30] Q.-J. Zhi, W.-P. Liu, R. Jiang, X.-N. Zhan, Y.-C. Jin, X. Chen, X. Yang, K.-Y. Wang, W. Cao, D.-D. Qi, J.-Z. Jiang, J. Am. Chem. Soc. 2022, 144, 21328-21336.
- [31] Y.-X. Liu, L. Li, Z.-Y. Sang, H. Tan, N. Ye, C.-L. Sun, Z.-Q. Sun, M.-C. Luo, S.-J. Guo, Nat. Synth. 2024, 4, 134-141.
- [32] X.-C. Zhang, S.-L. Cheng, C. Chen, X. Wen, J. Miao, B.-X. Zhou, M.-C. Long, L.-Z. Zhang, Nat. Commun. 2024, 15, 2649.
- [33] Y.-Z. Chen, R.-Y. Liu, Y.-Y. Guo, G. Wu, T. C. Sum, S.-W. Yang, D.-L. Jiang, Nat. Synth. 2024, 3, 998-1010.
- [34] Z.-H. Zhou, T.-Q. Ma, H.-Y. Zhang, S. Chheda, H.-Z. Li, K.-Y. Wang, S. Ehrling, R. Giovine, C. Li, A. H. Alawadhi, M. M. Abduljawad, M. O. Alawad, L. Gagliardi, J. Sauer, O. M. Yaghi, Nature 2024, 635, 96-101.
- [35] C. Gropp, T. Ma, N. Hanikel, O. M. Yaghi, Science 2020, 370, eabd6406.
- [36] T.-R. Liu, Q.-T. Tao, Y.-F. Wang, R.-G. Luo, J. Ma, J.-P. Lei, J. Am. Chem. Soc. 2024, 146, 18958-18966.



15213773, 0. Downloaded from https://onlinelibrary.wiley.com/doi/10.1002/anie.202505292 by Tianjin University Of, Wiley Online Library on [09.052025]. See the Terms and Conditions (https://onlinelibrary.wiley.com/terms-and-conditions)

on Wiley Online Library for rules of use; OA articles are governed by the applicable Creative Commons

- [37] L.-S. Sun, M. Lu, Z.-F. Yang, Z.-Y. Yu, X. Su, Y.-Q. Lan, L. Chen, Angew. Chem. Int. Ed. 2022, 61, e202204326; Angew. Chem. 2022, 134, e202204326.
- [38] M. Lu, S.-B. Zhang, M.-Y. Yang, Y.-F. Liu, J.-P. Liao, P. Huang, M. Zhang, S.-L. Li, Z.-M. Su, Y.-Q. Lan, *Angew. Chem. Int. Ed.* 2023, 62, e202307632; *Angew. Chem.* 2023, 135, e202307632.
- [39] M. Zhang, P. Huang, J.-P. Liao, M.-Y. Yang, S.-B. Zhang, Y.-F. Liu, M. Lu, S.-L. Li, Y.-P. Cai, Y.-Q. Lan, *Angew. Chem. Int. Ed.* 2023, 62, e202311999; *Angew. Chem.* 2023, 135, e202311999.
- [40] H. Dong, L. Fang, K.-X. Chen, J.-X. Wei, J.-X. Li, X. Qiao, Y. Wang, F.-M. Zhang, Y.-Q. Lan, Angew. Chem. Int. Ed. 2025, 64, e202414287.
- [41] K. Wu, X.-Y. Liu, P.-W. Cheng, Y.-L. Huang, J. Zheng, M. Xie, W.-G. Lu, D. Li, J. Am. Chem. Soc. 2023, 145, 18931–18938.
- [42] N.-Y. Liu, S.-L. Xie, Y.-X. Huang, J.-P. Lu, H.-J. Shi, S.-M. Xu, G.-G. Zhang, X. Chen, Adv. Energy Mater. 2024, 14, 2402395.
- [43] W. Li, X. Ding, B.-Q. Yu, H.-L. Wang, Z. Gao, X.-X. Wang, X.-L. Liu, K. Wang, J.-Z. Jiang, Adv. Funct. Mater. 2022, 32, 2207394.
- [44] Y.-K. Li, Z.-Y. Wang, Y.-Y. Jiang, C. Wu, C. Sun, Q.-R. Zhang, C. Zhang, H.-H. Fei, *Angew. Chem. Int. Ed.* 2024, e202415896.
- [45] X.-C. Lin, Y.-M. Wang, X. Chen, P.-Y. You, K.-M. Mo, G.-H. Ning, D. Li, Angew. Chem. Int. Ed. 2023, 62, e202306497; Angew. Chem. 2023, 135, e202306497.
- [46] T. Ozdemir, J. L. Bila, F. Sozmen, L. T. Yildirim, E. U. Akkaya, Org. Lett. 2016, 18, 4821–4823.
- [47] J.-N. Chang, S. Li, Q. Li, J.-H. Wang, C. Guo, Y.-R. Wang, Y.-F. Chen, S.-L. Li, Y.-Q. Lan, *Angew. Chem. Int. Ed.* 2024, 63, e202402458; *Angew. Chem.* 2024, 136, e202402458.
- [48] X.-X. Wang, X. Ding, Y.-C. Jin, D.-D. Qi, H.-L. Wang, Y.-S. Han, T.-Y. Wang, J.-Z. Jiang, Angew. Chem. Int. Ed. 2023, 62, e202302808; Angew. Chem. 2023, 135, e202302808.
- [49] Y.-N. Gong, W.-H. Zhong, Y. Li, Y.-Z. Qiu, L.-R. Zheng, J. Jiang, H.-L. Jiang, J. Am. Chem. Soc. 2020, 142, 16723–16731.
- [50] J. Li, H. Huang, W. Xue, K. Sun, X. Song, C. Wu, L. Nie, Y. Li, C. Liu, Y. Pan, H.-L. Jiang, D. Mei, C. Zhong, *Nat. Catal.* 2021, 4,719–729.
- [51] H.-L. Zheng, J.-Q. Zhao, Y.-Y. Sun, A.-A. Zhang, Y.-J. Cheng, L. He, X.-H. Bu, J. Zhang, Q.-P. Lin, J. Am. Chem. Soc. 2023, 145, 27728–27739.
- [52] Q.-X. Zhou, Y. Guo, Y.-F. Zhu, Nat. Catal. 2023, 6, 574–584.
- [53] G.-X. Lan, Y.-J. Fan, W.-J. Shi, E. You, S. S. Veroneau, W. Lin, Nat. Catal. 2022, 5, 1006–1018.
- [54] F.-M. Zhang, J.-L. Sheng, Z.-D. Yang, X.-J. Sun, H.-L. Tang, M. Lu, H. Dong, F.-C. Shen, J. Liu, Y.-Q. Lan, *Angew. Chem. Int. Ed.* 2018, 57, 12106–12110; *Angew. Chem.* 2018, 130, 12282–12286.
- [55] Y. Bai, L. Wilbraham, B. J. Slater, M. A. Zwijnenburg, R. S. Sprick, A. I. Cooper, J. Am. Chem. Soc. 2019, 141, 9063–9071.
- [56] Y.-Y. Wan, L. Wang, H.-X. Xu, X.-J. Wu, J.-L. Yang, J. Am. Chem. Soc. 2020, 142, 4508–4516.
- [57] S.-S. Li, C.-M. Gao, H.-H. Yu, Y.-W. Wang, S. Wang, W.-W. Ding, L.-N. Zhang, J.-H. Yu, Angew. Chem. Int. Ed. 2024, e202409925; Angew. Chem. 2024, 136, e202409925.

- [58] B. B. Rath, S. Krause, B. V. Lotsch, Adv. Funct. Mater. 2024, 34, 2309060.
- [59] Y.-N. Gong, J.-H. Mei, W.-J. Shi, J.-W. Liu, D.-C. Zhong, T.-B. Lu, Angew. Chem. Int. Ed. 2024, 63, e202318735; Angew. Chem. 2024, 136, e202318735.
- [60] Z.-F. Zhao, Y.-L. Zheng, C. Wang, S.-N. Zhang, J. Song, Y.-F. Li, S.-Q. Ma, P. Cheng, Z.-J. Zhang, Y. Chen, ACS Catal. 2021, 11, 2098–2107.
- [61] X.-L. Zu, X.-D. Li, W. Liu, Y.-F. Sun, J.-Q. Xu, T. Yao, W.-S. Yan, S. Gao, C.-M. Wang, S.-Q. Wei, Y. Xie, Adv. Mater. 2019, 31, 1808135.
- [62] D. Bohra, I. Ledezma-Yanez, G.-N. Li, W. de Jong, E. A. Pidko, W. A. Smith, Angew. Chem. Int. Ed. 2019, 58, 1345–1349; Angew. Chem. 2019, 131, 1359–1363.
- [63] S.-Q. Chang, Y. Feng, Y.-C. Zhao, Y.-H. Fu, H.-L. Jia, Y.-J. Gao, F.-M. Zhang, R. Ma, X.-Q. Lu, M.-H. Fan, W.-D. Zhu, ACS Appl. Mater. Interfaces 2024, 16, 13839–13848.
- [64] S.-Y. Wang, Z.-W. Ai, X.-W. Niu, W.-J. Yang, R. Kang, Z.-Y. Lin, A. Waseem, L. Jiao, H.-L. Jiang, Adv. Mater. 2023, 35, 2302512.
- [65] B. Wang, R. He, L.-H. Xie, Z.-J. Lin, X. Zhang, J. Wang, H.-L. Huang, Z.-J. Zhang, K. S. Schanze, J. Zhang, S.-C. Xiang, B.-L. Chen, J. Am. Chem. Soc. 2020, 142, 12478– 12485
- [66] Z.-A. Lan, G.-G. Zhang, X. Chen, Y.-F. Zhang, K. A. I. Zhang, X.-C. Wang, Angew. Chem. Int. Ed. 2019, 58, 10236–10240. Angew. Chem. 2019, 131, 10342–10346.
- [67] L. Liu, W.-D. Nie, H.-J. Wu, J.-R. Zhang, S.-S. Liang, H.-M. Zhu, Sci. China Mater. 2024, 67, 931–938.
- [68] H.-J. Wu, S.-S. Liang, W.-X. You, L. Liu, Y.-W. Guo, S.-J. Wang, L.-P. Song, Z.-H. Wang, H.-M. Zhu, J. Mater. Chem. C 2024, 12, 4825–4834
- [69] B. Song, W.-T. Song, Y.-H. Liang, Y. Liu, B.-W. Li, H. Li, L. Zhang, Y.-H. Ma, R.-Q. Ye, B.-Z. Tang, D. Zhao, Y. Zhou, B. Liu, Angew. Chem. Int. Ed. 2025, e202421248.
- [70] N.-Y. Huang, J.-Q. Shen, X.-W. Zhang, P.-Q. Liao, J.-P. Zhang, X.-M. Chen, J. Am. Chem. Soc. 2022, 144, 8676–8682
- [71] W.-T. Li, B. Han, Y.-H. Liu, J.-Y. Xu, H.-R. He, G.-G. Wang, J.-S. Li, Y.-X. Zhai, X.-L. Zhu, Y.-F. Zhu, Angew. Chem. Int. Ed. 2024, e202421356.
- [72] Z.-G. Zhou, L.-H. Li, B.-L. Li, J.-Y. Li, T.-Y. Liu, X. Huang, S.-B. Tang, H.-D. Qiu, W.-Z. Cai, S.-Y. Zhang, K. Li, G.-H. Xu, H.-Y. Zhen, Small 2023, 19, 2300013.
- [73] R.-M. Zhu, Y. Liu, W.-K. Han, J.-D. Feng, J.-F. Zhang, H. Pang, J.-W. Zhang, Z.-G. Gu, Angew. Chem. Int. Ed. 2025, 64, e202412890.

Manuscript received: March 05, 2025 Revised manuscript received: March 29, 2025 Accepted manuscript online: March 30, 2025 Version of record online:

Research Article



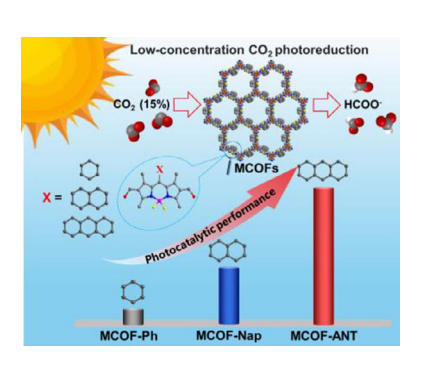
Research Article

MCOFs for CO₂ Photoreduction

C.-J. Lu, J.-H. Zhang, J.-H. Mei, Y.-N. Gong*, T.-B. Lu, D.-C. Zhong* _________ e202505292

Modulating the Chromophores of Metal-Covalent Organic Frameworks for Boosting Low-Concentration CO₂ Photoreduction

Three metal-covalent organic frameworks (MCOFs) with different chromophores were designed and synthesized, which exhibit efficient visible-light-driven reduction of low-concentration CO_2 to $HCOO^-$. Among which, MCOF-ANT with anthracene (ANT) group shows the highest $HCOO^-$ production rate of 1658 μ mol g^{-1} h^{-1} , which is 7.2 and 2.1 times higher than those of MCOF-Ph and MCOF-Nap with phenyl (Ph) and naphthalene (Nap) groups, respectively.



15217373, 0, Downloaded from https://onlinelibrary.wielyc.com/doi/10.002/anie.202505222 by Tianjin University Of, Wiley Online Library on 199.052025]. See the Terms and Conditions (https://onlinelibrary.wielyc.com/terms-und-conditions) on Wiley Online Library for rules of use; OA articles are governed by the applicable Creative Commons. Licenseque